Magnetoliposomes containing magnesium ferrite nanoparticles as nanocarriers for the model drug curcumin

Beatriz D. Cardoso,[a] Irina S. R. Rio,[a] Ana Rita O. Rodrigues,[a] Francisca C. T. Fernandes,[a] B. G. Almeida,[a] A. Pires,[b] A. M. Pereira,[b] J. P. Araújo,[b] Elisabete M. S. Castanheira[a] and Paulo J. G. Coutinho[a,†]

Magnesium ferrite nanoparticles, with diameters around 25 nm, were synthesized by coprecipitation method. The magnetic properties indicate a superparamagnetic behavior, with a maximum magnetization of 16.2 emu/g, a coercive field of 22.1 Oe and a blocking temperature of 183.2 K. These $MgFe_2O_4$ nanoparticles were used to produce aqueous and solid magnetoliposomes, with sizes below 130 nm. The potential drug curcumin was successfully incorporated in these nanosystems, with high encapsulation efficiencies (above 89%). Interaction by fusion between both types of drug-loaded magnetoliposomes (with or without PEGylation) and models of biological membranes was demonstrated, using FRET or fluorescence quenching assays. These results point to future applications of magnetoliposomes containing $MgFe_2O_4$ nanoparticles in cancer therapy, allowing combined magnetic hyperthermia and chemotherapy.

Introduction

Magnetic nanoparticles with superparamagnetic properties have attracted increased attention for applications in biomedicine, as they exhibit a strong magnetization only when an external magnetic field is applied.[1-3] Magnetoliposomes (liposomes entrapping magnetic nanoparticles) are promising therapeutic systems which can be guided and localized to specific sites by external magnetic field gradients[3-5] and used as an alternative to conventional chemotherapy through magnetically-controlled drug delivery and hyperthermia.[6-9]

In the past few years, rising attention has been given to the synthesis of ferrite nanoparticles without transition metals. Calcium and magnesium have been proposed to substitute transition metals in the crystalline structure of ferrite nanoparticles, as their ions are safely metabolized by the human body and may promote a higher biocompatibility.[9,10] In fact, *in vitro* cytotoxicity tests on T-cell lines showed that calcium ferrite nanoparticles are biocompatible at concentrations below 250 mg/mL, exhibiting an enhanced cell viability when compared to other ferrites.[11]

Magnesium ferrite nanoparticles are less sensitive to oxidation than magnetite and can be used as hyperthermia agents, as they display a large heating capacity which generates appropriate temperatures for hyperthermia.[12,13] Among all the techniques available for the synthesis of magnesium ferrite nanoparticles, the most used are sol gel, combustion and coprecipitation methods.[14-17] In order to obtain smaller particles, reverse coprecipitation and reverse micelle methods have been proposed,[14,18-19] to achieve nanoparticles with crystallite diameters around 20 nm.[14,18]

Curcumin is a natural polyphenolic compound with anti-inflammatory, antioxidant, antimicrobial and anticancer properties.[20] It was demonstrated that this compound has been involved in the mechanisms of regulation of target molecules, including transcription factors, growth factors, cytokines, enzymes and several genes that regulate cell proliferation and apoptosis.[21] Considering these properties and the lack of toxicity at high doses, curcumin has gained increased attention as a potential therapeutic agent for cancer, diabetes, allergies, neurodegenerative disorders, arthritis and other inflammatory diseases.[22-24] However, the therapeutic use of curcumin has been limited due to its hydrophobic character, implying low solubility and stability in aqueous media, and poor bioavailability (reduced absorption, rapid metabolism and systemic elimination). These obstacles have hampered the verification of the therapeutic efficacy of curcumin in clinical trials.[25] In order to overcome these limitations, the use of drug delivery systems, such as polymeric nanoparticles, micelles, liposomes and hydrogels, has been increased, to improve the bioavailability of the compound.[24-30]

In this work, novel magnetoliposomes containing biocompatible magnesium ferrite nanoparticles were tested as nanocarriers for curcumin as a model drug. These studies have demonstrated promising results for the use of these magnetoliposomes as drug nanocarrier systems, with potential applications in cancer therapy.

Experimental

All the solutions were prepared using spectroscopic grade solvents and ultrapure water (Milli-Q grade).

Preparation of magnesium ferrite nanoparticles

Magnesium ferrite nanoparticles were prepared by coprecipitation method. First, 10 mL of an aqueous solution containing 1.08 g of

[a.] *Centro de Física (CFUM), Universidade do Minho, Campus de Gualtar, 4710-057 Braga, Portugal.*
[b.] *IFIMUP/IN - Instituto de Nanociência e Nanotecnologia, R. Campo Alegre, 4169-007 Porto, Portugal*
[†] *Corresponding author; Phone: +351 253604321; Fax: +351 253604061; pcoutinho@fisica.uminho.pt*

Electronic Supplementary Information (ESI) available: Structures of the fluorescent-labeled lipids used in FRET assays; Results of Rietveld analysis; Size distribution of AMLs (by DLS); FRET assay for confirmation of the lipid bilayer in SMLs; Curcumin absorption and fluorescence in several solvents; Spectral overlap between curcumin emission and Nile Red absorption.

magnesium sulfate, 1.39 g of iron(II) sulfate heptahydrate and 200 µL of a 10% sulfuric acid solution were heated at 75 °C, under magnetic stirring, until a clear solution was obtained. Then, 1.02 g of potassium oxalate monohydrate were dissolved in 15 mL of warm deionized water. The two solutions were then mixed, under vigorous stirring, at 90 °C. After 15 minutes, the solution was cooled to room temperature. The precipitated nanoparticles were washed by several cycles of centrifugation and redispersion in water. Finally, the nanoparticles were calcined at 600 °C for 3 hours.

Preparation of magnetoliposomes

For magnetoliposomes preparation, the lipids egg yolk phosphatidylcholine (Egg-PC), dipalmitoyl phosphatidylcholine (DPPC) (from Sigma-Aldrich), and 1,2-distearoyl-*sn*-glycero-3-phosphoethanolamine-*N*-[methoxy(polyethylene glycol)-2000] (ammonium salt) (DSPE-PEG2000, from Avanti Polar Lipids) were used. For aqueous magnetoliposomes preparation, a 10 mM lipid solution in ethanol was injected, under vigorous vortexing, to a dispersion of magnetic nanoparticles in ultrapure water (pH=7), above the melting transition temperature of the lipids, 41 °C for DPPC and -18 °C for Egg-PC (ethanolic injection method).[31] At this pH, the nanoparticles are below their point of zero charge (a PZC value of 8.4 was reported for similar $MgFe_2O_4$ nanoparticles also calcined at 600 °C)[32] and thus are expected to be well dispersed at the time of injection. After encapsulation, an ultracentrifugation was performed to remove all the non-encapsulated nanoparticles.

Solid magnetoliposomes (SMLs) were prepared by a method previously developed.[33,34] First, 10 µL of the synthesized $MgFe_2O_4$ NPs were dispersed in 3 mL of water and centrifuged. Then, the deposited particles were dispersed in 10 µL water in an ultrasonicator, for one minute at 189 W, and 3 mL of chloroform were added to the aqueous dispersion of NPs. After vigorous agitation, 165 µL of a 20 mM solution of dipalmitoylphosphatidylcholine (DPPC) were added under vortexing, to form the first lipid layer of the SMLs. The particles were washed twice by magnetic decantation with pure water, in order to remove the lipid that was not attached to the NPs. The second lipid layer was then formed by the injection of 165 µL of a lipid solution (20 mM), under vortexing, in a 3 mL aqueous dispersion of the particles with the first layer. The resulting SMLs were then washed and purified with ultrapure water by centrifugation. The formation of a lipid bilayer around the prepared magnesium ferrite nanoparticles was confirmed by Förster Resonance Energy Transfer (FRET) measurements, using the labeled lipids NBD-C_{12}-HPC (1-palmitoyl-2-{12-[(7-nitro-2-1,3-benzoxadiazol-4-yl)amino]hexanoyl}-*sn*-glycero-3-phosphocholine) and Rhodamine B-DOPE (*N*-(lissamine Rhodamine B sulfonyl)-1,2-dioleoyl-*sn*-3-phosphatidylethanolamine (ammonium salt)), both from Avanti Polar Lipids (structures in Figure S1 of Supplementary Information), as previously described.[33,34]

Curcumin was entrapped in aqueous magnetoliposomes by the co-injection method, while in solid magnetoliposomes the drug was incorporated by injection of an ethanolic solution together with the formation of the second lipid layer, as already reported for the incorporation in magnetoliposomes of several new antitumor compounds.[34-36]

Preparation of Giant Unilamellar Vesicles (GUVs)

Soybean lecithin (*L*-α-Phosphatidylcholine), from Sigma-Aldrich, was used for GUVs preparation, using a procedure described by Tamba *et al*.[37,38] 100 µL of soybean lecithin solution (1 mM) were dried under an argon stream to produce a thin and homogeneous lipid film. 40 µL of water were added to the film and it was incubated at 45 °C for 30 minutes. Then, 3 mL of 0.1 M glucose aqueous solution were added and the resulting mixture was again incubated at 37 °C for 2 hours. Finally, after incubation, the GUVs suspension was centrifuged at 14000 g for 30 minutes at 20 °C, to remove multilamellar vesicles and lipid aggregates.

Spectroscopic measurements

General methods. Absorption spectra were recorded in a Shimadzu UV-3101PC UV-Vis-NIR spectrophotometer. Fluorescence measurements were performed using a Fluorolog 3 spectrofluorimeter, equipped with double monochromators in both excitation and emission, Glan-Thompson polarizers and a temperature controlled cuvette holder. Fluorescence spectra were corrected for the instrumental response of the system.

The steady-state fluorescence anisotropy, *r*, taken as the average value in an appropriate spectral range, is calculated by

$$r = \frac{I_{VV} - G I_{VH}}{I_{VV} + 2G I_{VH}} \quad (1)$$

where I_{VV} and I_{VH} are the intensities of the emission spectra obtained with vertical and horizontal polarization, respectively (for vertically polarized excitation light), and $G = I_{HV}/I_{HH}$ is the instrument correction factor, where I_{HV} and I_{HH} are the emission intensities obtained with vertical and horizontal polarization (for horizontally polarized excitation light).

FRET measurements. FRET efficiency, Φ_{RET}, defined as the proportion of donor molecules that have transferred their excess energy to acceptor molecules, can be obtained by taking the ratio of the donor integrated fluorescence intensities in the presence of acceptor (F_{DA}) and in the absence of acceptor (F_D) (eqn. 2),[39]

$$\Phi_{RET} = 1 - \frac{F_{DA}}{F_D} \quad (2)$$

The distance between donor and acceptor molecules can be determined through the FRET efficiency (eqn. 2),

$$r_{AD} = R_0 \cdot \left[\frac{1-\Phi_{RET}}{\Phi_{RET}}\right]^{1/6} \quad (3)$$

where R_0 is the Förster radius (critical distance), that can be obtained by the spectral overlap, J(λ), between the donor emission and the acceptor absorption, according to equations (4) and (5) (with R_0 in Å, λ in nm, $\varepsilon_A(\lambda)$ in M^{-1} cm^{-1}),[39]

$$R_0 = 0.2108\left[k^2 \Phi_D^0 n^{-4} J(\lambda)\right]^{1/6} \quad (4)$$

$$J(\lambda) = \int_0^\infty I_D(\lambda)\varepsilon_A(\lambda)\lambda^4 d\lambda \quad (5)$$

where $k^2 = 2/3$ is the orientational factor assuming random orientation of the dyes, Φ_D^0 is the fluorescence quantum yield of the donor in the absence of energy transfer, *n* is the refraction index of the medium, $I_D(\lambda)$ is the fluorescence spectrum of the

donor normalized so that $\int_0^\infty I_D\,(\lambda)d\lambda = 1$, and $\varepsilon_A(\lambda)$ is the molar absorption coefficient of the acceptor.

For determination of fluorescence quantum yield of NBD-C_{12}-HPC (energy donor) in magnetoliposomes containing mangnesium ferrite nanoparticles, this fluorescent labeled lipid incorporated in lipid membranes was used as reference, Φ_r=0.32 at 25 °C, as reported by Invitrogen.[40]

Structural characterization

Scanning Electron Microscopy (SEM). SEM images of magnesium ferrite nanoparticles and solid magnetoliposomes were recorded using a Scanning Electron Microscope FEI - Nova 200 NanoSEM, operating in transmission mode (STEM). In the case of SMLs, a negative staining was employed. For that, a 2% aqueous solution of ammonium molybdate tetrahydrate was prepared. Then, 20 µL of sample and 20 µL of staining solution were mixed and a drop of this mixture was placed onto a Formvar grid, held by tweezers. After 20 seconds, almost all the solution was removed with filter paper and left dry. The processing of STEM images was performed using ImageJ software. It consisted in enhancing local contrast followed by automatic local thresholding and particle analysis. The area of each particle allowed an estimation of the particle diameter. The resulting histograms were fitted to Gaussian distributions.

X-Ray Diffraction (XRD) and DLS measurements. X-Ray Diffraction (XRD) analyses were performed using a conventional Philips PW 1710 diffractometer, operating with CuK_α radiation, in a Bragg-Brentano configuration.

Liposomes mean diameter and size distribution (polydispersity index) were measured using a Dynamic Light Scattering (DLS) equipment (NANO ZS Malvern Zetasizer) at 25 °C, using a He-Ne laser of λ=632.8 nm and a detector angle of 173°. Five independent measurements were performed for each sample.

Magnetic measurements

General methods. Magnetic measurements were performed at room temperature in a Superconducting Quantum Interference Device (SQUID) magnetometer (Quantum Design MPMS5XL), using applied magnetic fields up to 5.5 T.

Temperature dependence of the magnetization and magnetic hysteresis cycles. The temperature dependence of the magnetization was measured in the temperature range from 5 K to 380 K. The curves were obtained by initially cooling the sample under an applied magnetic field of *H* = 100 Oe (field cooled, *FC*) and then measuring its magnetization with increasing temperature (applied field of *H* = 50 Oe). Subsequently, after reaching 350 K, the sample was recooled, this time with no applied magnetic field (zero-field-cooled, *ZFC*) and the magnetization measurements were again performed with increasing temperature, under the same magnetic field of *H* = 50 Oe. From the behavior of the *FC* and *ZFC* curves, the blocking temperature (T_B) of the superparamagnetic nanoparticles can be obtained.[41] The magnetization hysteresis loop measurements were made by fixing the temperature and measuring the magnetization at a series of different applied magnetic fields. This type of study gives information about the maximum magnetization and the degree at which the sample remains magnetized when the applied field is removed, and how easily the sample magnetization can be reversed, the so-called coercive field.

Curcumin Encapsulation Efficiency

The encapsulation efficiency, *EE*(%), of curcumin in magnetoliposomes was determined through fluorescence emission measurements. After preparation, drug-loaded magnetoliposomes (MLs) were subjected to centrifugation at 10000 rpm for 60 minutes. The supernatant was pipetted out and its fluorescence was measured, allowing to determine the drug concentration using a calibration curve previously obtained. Three independent measurements were performed for each system and standard deviations (SD) were calculated. The encapsulation efficiency was determined using the following equation:

$$EE(\%) = \frac{(total\ amount - amount\ of\ non\ encapsulated\ drug)}{total\ amount} \times 100 \quad (6)$$

Results and discussion

Nanoparticles characterization

XRD analysis. XRD measurements allowed confirming the synthesis of the magnesium ferrite nanoparticles. A calcination process at 600 °C was needed to obtain a crystalline phase. All the characteristic peaks for a pure crystalline phase of magnesium ferrite spinel,[19,42] marked by their indices ($MgFe_2O_4$, space group F d -3 m:1, CIF 1011245, are shown in Figure 1. For Rietveld analysis using FullProf software,[43] the background was defined by a linear interpolation between a set of points at fixed scattering angles, but with fitted intensities. It was impossible to obtain good fits when considering a direct spinel structure of type $Mg^{Td}Fe_2^{Oh}O_4$ as indicated in CIF 1011245. As the peaks (2 2 0) and (4 4 0) have increased intensities when compared to that of the main peak, (3 1 1), inclusion of preferential orientation correction at (1 1 0) plane[36] resulted in a small but insufficient improvement (Table S1 in Supplementary Information). Considering that the spinel structure has a cation ordering according to $Mg^{Td}_{(1-i)}Fe^{Td}{}_iMg^{Oh}{}_iFe^{Oh}_{(2-i)}O_4$, the Rietveld optimization resulted in a reasonable fit for a degree of inversion, *i*, of 0.897, with χ^2 = 2.92 and a R_F factor of 6.8. The use of preferential orientation correction improved the fitting quality parameters to χ^2 = 2.35 and R_F = 5.03, with *i* = 0.825. The corresponding average size is 33 nm.

The obtained values for the degree of inversion are within the reported values of 0.56 [44] and 0.9,[45] and depend on the preparation method and crystallite size, as it was demonstrated for the case of $ZnFe_2O_4$.[46]

Scanning Electron Microscopy. STEM images of the nanoparticles prepared by the procedure here described revealed generally spherical nanoparticles uniform in size, with a size distribution of 24.5 ± 8.7 nm (Fig. 2). This size compares well with the ones reported by Chandradass *et al.*,[14] who prepared nanopowders with 19.6 ± 2 nm diameter (although by a different method, the reverse microemulsion), and also by Kanagesan *et al.*,[15] who obtained nanoparticles with diameters

around 20 nm. Maensiri and coworkers[42] also prepared $MgFe_2O_4$ nanoparticles (incorporated in electrospun polyvinylpyrrolidone (PVP) nanofibers) with sizes increasing from 15 ± 4 nm to 24 ± 3 nm, when the calcination temperature was raised from 500 to 800 °C. Here, the size distribution obtained by STEM is roughly in accordance with the one estimated by XRD.

UV-Visible absorption spectra. The UV-Visible absorption (or transmission) spectrum of the synthesized magnesium ferrite nanoparticles allows obtaining the optical band gap using a Tauc plot,[47] which corresponds to equation (7):

$$(\alpha h\nu)^n \propto (h\nu - E_g) \quad (7)$$

where α is the absorption coefficient that is proportional to the absorbance, *n* is an exponent that depends on the nature of the transition (being *n*=2 for a direct semiconductor and *n*=1/2 for an indirect one), and E_g is the optical band gap.
A linear relation was only obtained for *n*=2 (Fig. 3) indicating that $MgFe_2O_4$ behaves as a direct semiconductor.

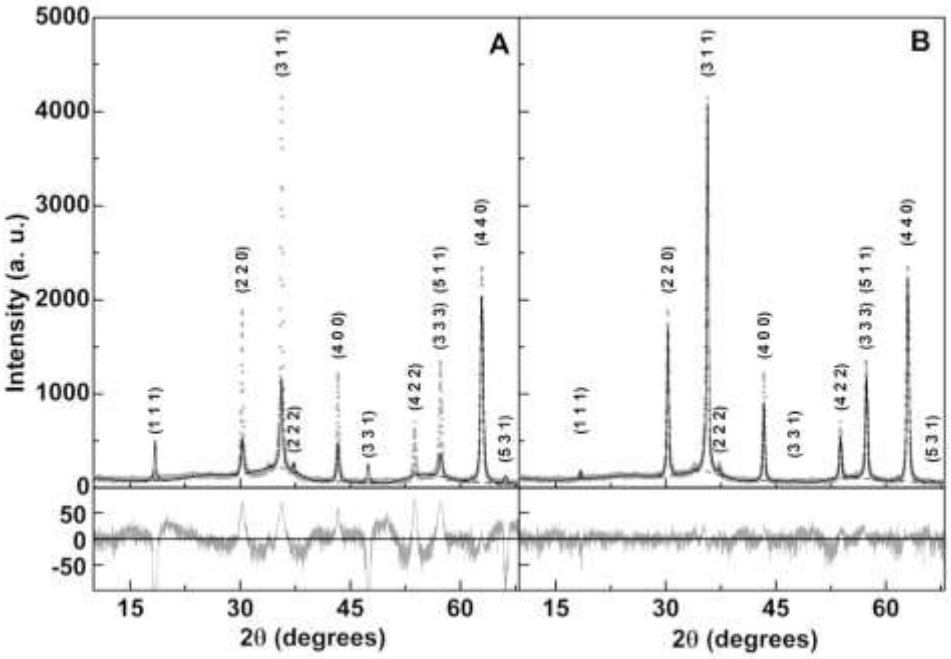

Fig. 1 XRD pattern of the $MgFe_2O_4$ nanoparticles calcined at 600 °C and Rietveld analysis using preferential orientation correction at the (1 1 0) plane, a fitted background represented by a dashed line and considering either direct (**A**) or 82.5% inverted (**B**) spinel structure.

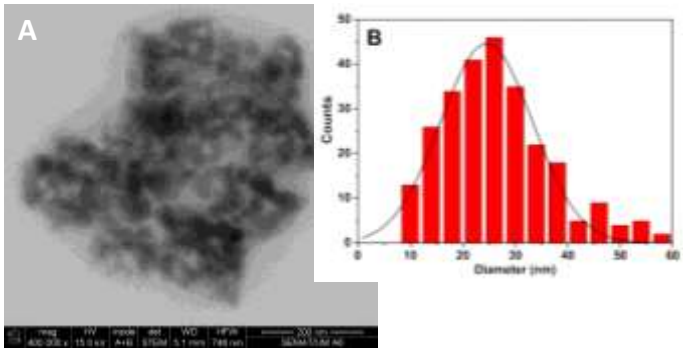

Fig. 2 A. STEM image of $MgFe_2O_4$ nanoparticles. **B.** Particles size histogram of image A and fitting to a Gaussian distribution.

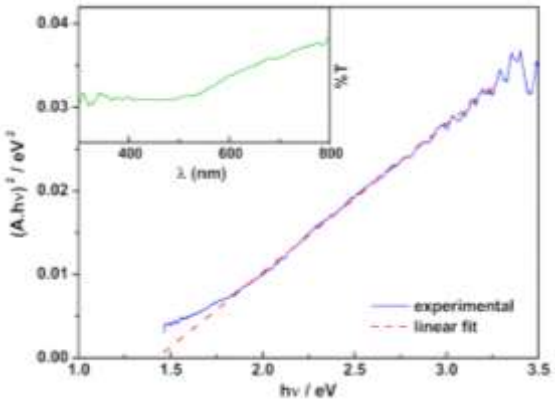

Fig. 3 Tauc plot for magnesium ferrite nanoparticles. Inset: UV-Visible transmission spectra of NPs dispersed in water.

A band gap of 1.41 eV was estimated from the intercept of Tauc plot (Fig. 3), in good agreement with the results of Manikandan *et al.,*[48] but somewhat lower than the value of 2.0 eV reported by Kim and coworkers.[49]

Magnetic properties. Figure 4 displays the temperature dependence of the magnetization measured with zero field cooled (*ZFC*) and field cooled (*FC*) curves in the temperature range from 5 K to 350 K. The blocking temperature (T_B) distributions of $MgFe_2O_4$ nanoparticles were determined by the temperature derivative of the difference between the *ZFC* and *FC* magnetization curves (inset of Fig. 4). Here, the maximum (T_{max} = 183.23 K), corresponds to the blocking temperature of the main size distribution.[50] This method has shown to be more accurate than the one that considers T_B as the maximum of the *ZFC* curve,[51] as the dipolar interactions result in a shift of the *ZFC* maximum to higher temperatures.

Figure 5 shows the magnetization hysteresis cycle of magnesium ferrite nanoparticles. The maximum magnetization value at 50 kOe, 16.2 emu/g, is slightly smaller than the one obtained by Maensiri *et al.*[42] for $MgFe_2O_4$ nanoparticles incorporated in electrospun PVP nanofibers also calcined at 600 °C, but higher than those reported by Kaur *et al.*[16] for NPs prepared by different chemical methods (including coprecipitation). As previously observed by Chandradass *et al.*[14] and Maensiri *et al.*,[42] a saturation was not attained in the magnetization hysteresis loop, maybe due to the presence of surface defects. Chandradass and coworkers[14] prepared magnesium ferrite NPs with a maximum magnetization of M_s=12.9 emu/g also by coprecipitation. Maensiri and coworkers[42] reported that calcination at higher temperatures (700 – 800 °C) of $MgFe_2O_4$/PVP nanocomposites causes an increase in the maximum magnetization, but also in both H_c and M_r, with the loss of superparamagnetism of the NPs (for superparamagnetic nanoparticles, $M_r/M_s < 0.1$).

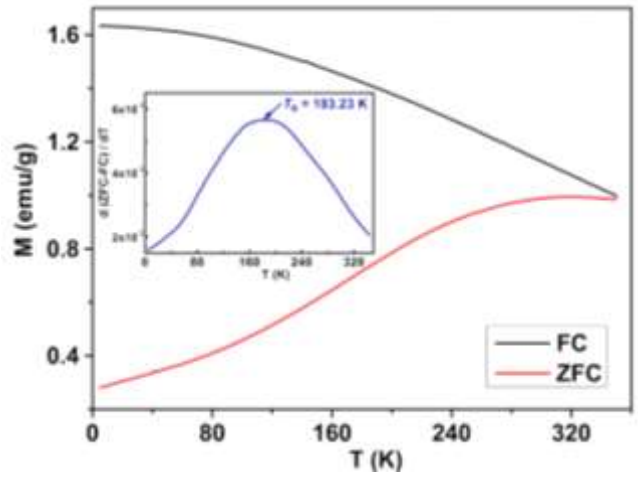

Fig. 4 Temperature dependence of the magnetization (*ZFC* and *FC*) of $MgFe_2O_4$ nanoparticles over the temperature range 5 – 350 K, with H=50 Oe. Inset: Temperature derivative of the difference between *ZFC* and *FC* magnetization curves.

A decrease of the magnetization of oxide nanoparticles can be caused by surface effects, like a surface disordered or a magnetically dead surface layer.[52] Moreover, the relative amount of Fe^{3+} ions at A (T_d) and B (O_h) positions in the nanocrystal may strongly decrease the maximum magnetization, since the spins of ions in A and B sites magnetize oppositely the corresponding sublattices in the incomplete inverse spinel structure.[53]

Nevertheless, the nanoparticles here obtained stand out considering the low coercive field (H_c) and residual magnetization (M_r), indicating that most of the nanoparticles shows a superparamagnetic behavior (M_r/M_s=0.02, Table 1).

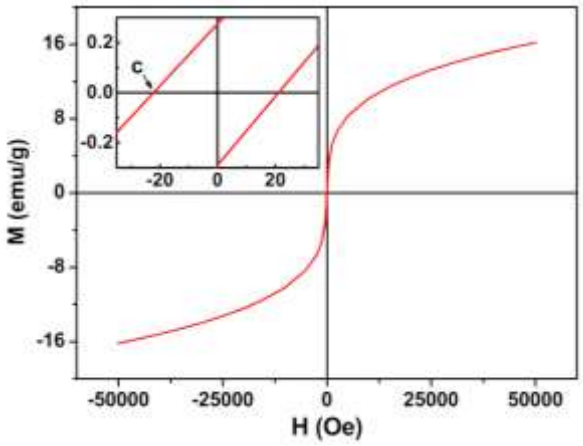

Fig. 5 Magnetization hysteresis loop of $MgFe_2O_4$ NPs measured at room temperature. Inset: Enlargement of the loop, in the low field region.

Table 1. Coercive field (H_C), maximum magnetization (M_s), remnant magnetization (M_r) and ratio M_r/M_S for magnesium ferrite NPs. SQUID data available at https://doi.org/10.5061/dryad.482q2rh

H_C (Oe)	M_S (emu/g)	M_r (emu/g)	M_r/M_S
22.1	16.16	0.26	0.02

The critical size (in zero or a small field), D, for superparamagnetic behaviour can be obtained by[54]

$$D = \sqrt[3]{\frac{6k_B T \ln(t_m f_0)}{\pi K}} \quad (9)$$

where K is the anisotropy constant, f_0 is the frequency constant (10^9 Hz), k_B is the Boltzmann's constant, T the absolute temperature and t_m is the time of measurement. An anisotropy constant of 0.61×10^5 erg cm^{-3} is reported for $MgFe_2O_4$,[55] leading to a critical size for superparamagnetic behaviour of about 33 nm, at room temperature. Thus, the size of $MgFe_2O_4$ nanoparticles here obtained (both by XRD and SEM) is in accordance with the superparamagnetic behavior predicted by SQUID measurements.

The inductive heating capability of magnetic nanoparticles, under an alternating current magnetic field, is directly proportional to the area of the hysteresis cycle and thus rises as the coercive field is increased, decreasing with the diminution of the maximum magnetization.[56] Here, the significant coercive field (22.1 Oe, Table 1) compensates the lower maximum magnetization of $MgFe_2O_4$ nanoparticles when compared to that of other ferrites (nickel, manganese, iron or cobalt),[33,34,50] and points to a possible application of these nanoparticles in magnetic hyperthermia therapies. The negative effect of the lower M_s value of $MgFe_2O_4$ on the inductive heating capability can also be compensated by the occurrence of small clusters of magnetic nanoparticles, that

originate an additional and significant heating capacity, enough to reach therapeutic temperatures, as already reported.[57]

Comparing with transition metal ferrite nanoparticles previously incorporated in solid and aqueous magnetoliposomes (namely, nickel ferrite and manganese ferrite),[33-35] magnesium ferrite nanoparticles have the advantage of guaranteed biocompatibility,[9,10] not compromising the superparamagnetic behaviour. Considering magnetite, despite the reported biocompatibility, it has been shown that these nanoparticles are sensitive to oxidation, being transformed into maghemite in the presence of oxygen.[58] Moreover, it has been described that iron oxide nanoparticles induce the production of reactive oxygen species (ROS) in mammalian cells,[59] causing severe DNA and protein damage and inflammatory responses.[60,61] Therefore, magnesium ferrite nanoparticles can be advantageous, avoiding these undesirable effects.

Characterization of magnetoliposomes

DLS and SEM measurements. Two types of magnetoliposomes were obtained, solid magnetoliposomes (SMLs) and aqueous magnetoliposomes (AMLs). The biocompatibility of magneto-liposomes (containing $MnFe_2O_4$ nanoparticles) of the same lipids and prepared by the same techniques was previously reported.[35] Aqueous magnetoliposomes were prepared by ethanolic injection of the lipids[31] in the aqueous ferrofluid. This methodology was chosen because it is very advantageous for hydrophobic drugs[62] (as is the case of curcumin, exhibiting a very limited solubility in aqueous media), which can be loaded into magnetoliposomes by coinjection. Dynamic Light Scattering (DLS) measurements were used to characterize aqueous magnetoliposomes containing $MgFe_2O_4$ nanoparticles. These systems exhibit diameters of 122 ± 19 nm (size distribution in Fig. S2 of Supplementary Information), with a low polydispersity (below 0.2). This result is similar to the one reported recently for AMLs of the same lipid containing iron oxide nanoparticles,[36] however being somewhat higher than those of AMLs containing transition metal ferrites.[33,34] For enhanced permeability and retention (EPR) effect of loaded drugs, the size of magnetoliposomes must be small, and a successful extravasation into tumors has been shown to occur for nanocarriers with sizes below 200 nm.[63]

Solid magnetoliposomes (SMLs) were obtained by coverage of a cluster of magnesium ferrite NPs by the phospholipid DPPC, using the method previously developed for Ni ferrite and Mn ferrite nanoparticles.[33,34] Following the same procedure, the formation of the lipid double layer was proven by FRET, Rhodamine B-DOPE labeling the first lipid layer of magnetoliposomes and the second lipid layer containing NBD-C_{12}-HPC. Upon double layer formation, a strong energy transfer is observed from NBD (donor) to Rhodamine B (acceptor), with a FRET efficiency of 73% (Fig. S3 in Supplementary Information). Using eqns. (3) to (5), a donor-acceptor distance of 3.8 nm proves the formation of the lipid bilayer around the nanoparticles cluster, which has a typical thickness between 7 and 9 nm.[64] SEM images of SMLs (obtained with a negative staining) revealed that the synthesized solid magnetoliposomes present diameters slightly above 100 nm (Fig. 6). Fig. 6A exhibits several magnetoliposomes containing nanoparticles clusters (with one smaller cluster in the middle). A single magnetoliposome is observed in Fig. 6B. The size obtained is slightly smaller than those of SMLs of DPPC containing $MnFe_2O_4$ and Fe_3O_4 nanoparticles.[35,36] As reported previously,[35] the interest in using a DPPC bilayer in SMLs is the melting transition temperature of this phospholipid (T_m = 41 °C),[65] approaching the temperatures used in mild hyperthermia therapy. An additional increase in membrane fluidity is expected upon lipid phase transition (from the gel to the liquid crystalline phase), with a potential enhancement in drug release capability of the solid magnetoliposomes.

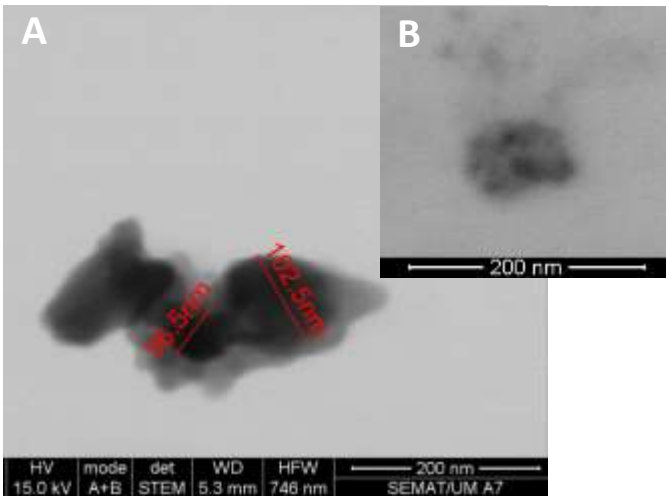

Fig. 6 SEM images of solid magnetoliposomes (SMLs) containing magnesium ferrite nanoparticles (obtained with a negative staining).

Incorporation of curcumin in AMLs and SMLs. The potential drug curcumin is fluorescent in several polar and non-polar solvents (Fig. S4 in Supplementary Information). The absorption and emission bands of curcumin can be attributed to the enol-keto tautomer,[66] while in water/ethanol and water/acetonitrile mixtures the existence of the diketo tautomer was reported.[67,68] Large spectral red shifts, band enlargement and loss of vibrational structure are observed for the emission in polar media (Fig. S4), this behavior being attributed to a strong intramolecular charge transfer mechanism in the excited state, as well as to hydrogen bonding in protic solvents.[68]

Curcumin was loaded into both AMLs and SMLs containing $MgFe_2O_4$ NPs. Figure 7 shows the emission spectra of this dye in AMLs, SMLs and liposomes without magnetic nanoparticles (but with the same concentration of compound), which allow concluding that curcumin is fully incorporated in these nanosystems, as it is non-emissive in aqueous media. It is also possible to observe a quenching effect of the fluorophore emission by the magnetic nanoparticles, much more pronounced in SMLs, similarly to what was reported for other potential drugs and different magnetic nanoparticles.[34-36] Also, a small red shift in emission is detected in liposomes and AMLs, when compared to SMLs, indicating a more hydrated environment for curcumin in the latter nanosystems, which was expected considering that SMLs do not contain an interior aqueous volume.

Fluorescence anisotropy measurements (Table 2) were performed to confirm that curcumin is fully incorporated in both types of

magnetoliposomes, located mainly in the lipid bilayer. First, the anisotropy values are generally high at room temperature, but smaller (as expected) the one measured in the highly viscous solvent glycerol (viscosity around 1000 cP), which is much more viscous than lipid membranes, the latter possessing viscosities of 100-200 cP.[69,70] Also, the transition from the gel phase (at 25 °C) to the liquid crystalline phase (at 55 °C) of DPPC is detected by curcumin through a decrease in its fluorescence anisotropy; finally, anisotropy values are roughly similar in magnetoliposomes and neat liposomes. However, the anisotropy in SMLs at room temperature is smaller than the one in AMLs or liposomes. Although possible differences in the fluorophore excited-state lifetime can occur, it is known that lipid membrane viscosity decreases from the surface to the interior.[71,72] This can justify the lower *r* value in SMLs, indicating that curcumin is located deeply in SMLs membranes.

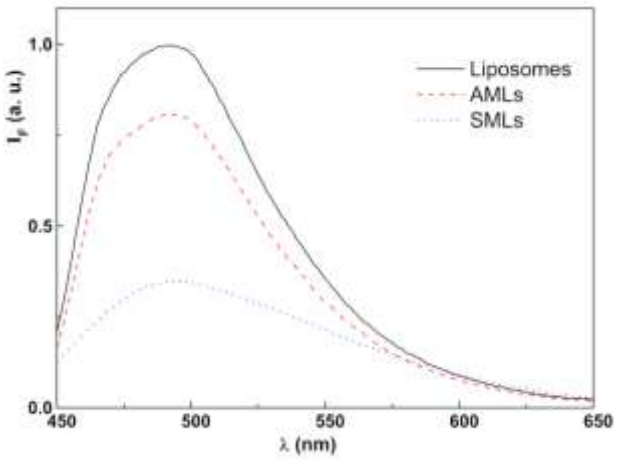

Fig. 7 Fluorescence spectra (λ_{exc}=420 nm) of curcumin (3×10^{-6} M) in liposomes (without magnetic NPs), aqueous magnetoliposomes (AMLs) and solid magnetoliposomes (SMLs) containing magnesium ferrite nanoparticles.

Table 2. Steady-state fluorescence anisotropy (*r*) values for curcumin in liposomes (for comparison), aqueous magnetoliposomes (AMLs) and solid magnetoliposomes (SMLs). Spectral data available at https://doi.org/10.5061/dryad.482q2rh

	Lipid formulation	Temperature	*r* [a]
Liposomes	Egg-PC	25 °C	0.331
	DPPC	25 °C	0.287
		55 °C	0.119
AMLs	Egg-PC	25 °C	0.328
	DPPC	25 °C	0.291
		55 °C	0.147
SMLs	DPPC	25 °C	0.141
		55 °C	0.113

[a] Anisotropy of curcumin in glycerol is 0.365 at 25 °C.[73]

The curcumin encapsulation efficiencies in both AMLs and SMLs are presented in Table 3. Values of encapsulation efficiencies are larger than 89%, the lowest *EE%* being observed in solid magnetoliposomes. These high encapsulation efficiencies point to a promising use of these nanocarriers for hydrophobic drugs and as agents for simultaneous chemotherapy and magnetic hyperthermia.

Table 3. Encapsulation efficiencies (*EE%*) and standard deviations (SD) of curcumin in aqueous and solid magnetoliposomes. Original data available at https://doi.org/10.5061/dryad.482q2rh

System	*EE% ± SD*
AMLs (Egg-PC)	98.4 ± 1.4
SMLs (DPPC)	89.5 ± 8.0

These results also show the suitability of the ethanolic injection method for the preparation of curcumin-loaded magnetoliposomes. Using the same methodology, Jaafar-Maalej *et al.*[62] reported encapsulation efficiencies in liposomes above 87% for another hydrophobic drug (beclomethasone dipropionate, BDP), attaining 100% in some cases. The *EE%* values in Table 3 are also similar to the ones previously reported for magnetoliposomes containing new antitumor thienopyridine derivatives.[35]

Taking advantage of curcumin fluorescence, the non-specific interaction of both types of drug-loaded magnetoliposomes with giant unilamellar vesicles (GUVs) was monitored, using GUVs as models of cell membranes,[37,38] allowing to investigate the possibility of drug release by fusion. For that purpose, Förster Resonance Energy Transfer (FRET) was employed, using curcumin as the energy donor and the hydrophobic dye Nile Red (widely used as lipid probe)[74-77] as the energy acceptor. This is a very favorable donor-acceptor pair, as evaluated by the spectral overlap between curcumin emission and Nile Red absorption (Fig. S5 in Supplementary Information). Therefore, a high FRET efficiency is expected if the donor-acceptor distance is below 100 Å, this efficiency strongly decreasing with the increase in the donor-acceptor distance.[39]

If magnetoliposomes interact with model membranes (GUVs) and fusion between them occurs, a larger membrane will be created and an increase in the donor-acceptor distance will be verified, with a corresponding decrease in the energy transfer efficiency. This was verified for aqueous magnetoliposomes, when these nanosystems were loaded with both curcumin and Nile Red (Fig. 8). Two emission bands, the first due to curcumin fluorescence (λ_{max}=510 nm) and the second due to Nile Red emission (λ_{max}=630 nm) are detected, if only curcumin is excited (Fig. 8A). After interaction with GUVs, an increase in the curcumin (donor) fluorescence band and a decrease of the Nile Red (acceptor) emission band is observed, proving the diminution of FRET efficiency, as a result of membrane fusion.

In order to prevent the adsorption of plasma proteins (opsonization) and promote the shielding from proteolytic enzymes, increasing the retention time in the circulation system,[78,79] PEGylation of Egg-PC aqueous magnetoliposomes was carried out, aiming at obtaining longer-circulating nanosystems in the blood flow. This was achieved by using 5% of DSPE-PEG-2000 in the lipid composition. It has been reported that the coating with PEG is effective in increasing the circulation time of magnetite nanoparticles covered with oleic acid[79] and of magnetoliposomes.[6] However, recently it was also shown that PEGylation can reduce the

interaction of magnetoliposomes with cells, with a corresponding decrease in the degree of internalization.[80]

Fluorescence anisotropy of curcumin in PEGylated Egg-PC AMLs (r=0.341) is very similar to the one in non-PEGylated magnetoliposomes of the same lipid (Table 2). The interaction with GUVs was equally investigated (Fig. 8B). It was observed a diminution of FRET efficiency, indicating fusion with GUVs, however in a lower extent than for non-PEGylated systems. These results point to a higher resistance of PEGylated AMLs to interaction with GUVs, but still maintaining some fusogenic capability.

In the case of solid magnetoliposomes, the emission of curcumin in SMLs incorporating also Nile Red is completely suppressed, as it suffers fluorescence quenching from the nanoparticles and also by energy transfer to the acceptor Nile Red. Therefore, an assay was made with SMLs containing only curcumin. Upon interaction with GUVs, an unquenching effect of the drug fluorescence is detected, proving membrane fusion (Fig. 9A). A similar effect upon interaction with model membranes was detected previously for SMLs containing manganese ferrite nanoparticles[34] and magnetite nanoparticles[36] loaded with other antitumor drugs. A small red shift of curcumin fluorescence after interaction with GUVs may indicate, as previously referred, a slightly more hydrated environment felt by the drug after membrane fusion.

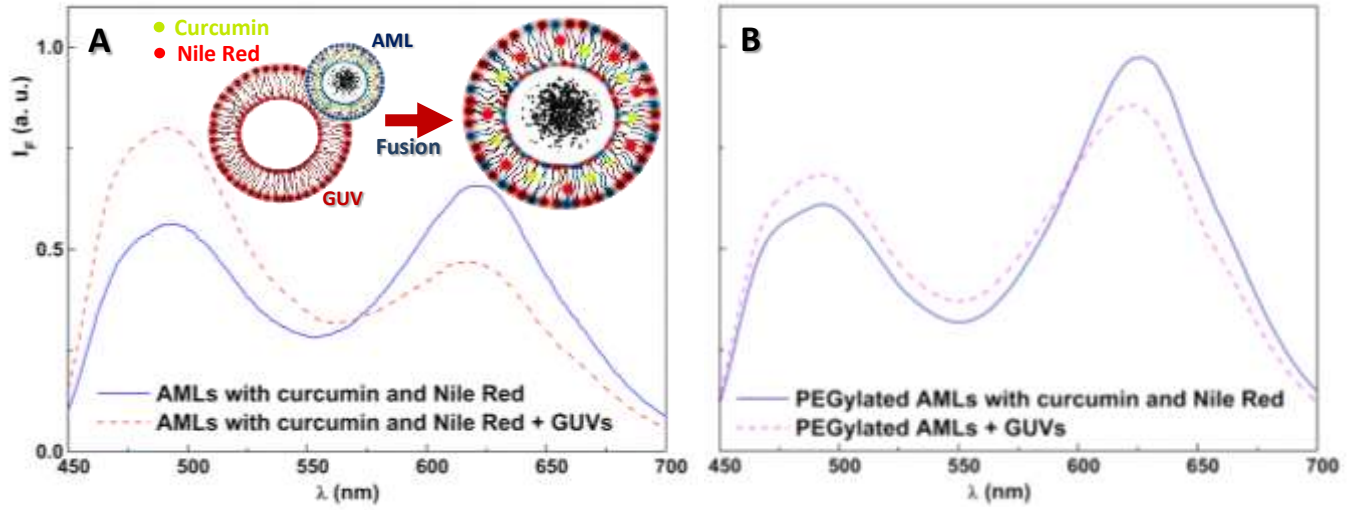

Fig. 8 Fluorescence spectra (λ_{exc}=420 nm) of aqueous magnetoliposomes (AMLs) based on $MgFe_2O_4$ NPs and containing both curcumin and Nile Red, before and after interaction with GUVs. **A.** AMLs of egg phosphatidylcholine. **B.** PEGylated AMLs. Inset: Schematic representation of membrane fusion between AMLs and GUVs.

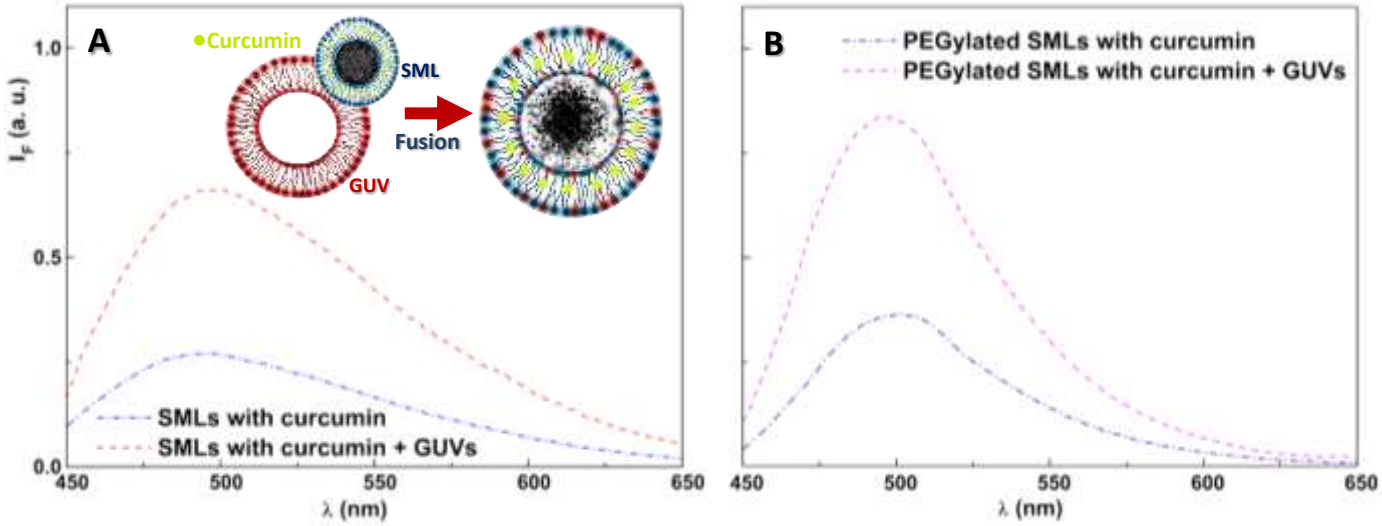

Fig. 9 Fluorescence spectra (λ_{exc}=420 nm) of curcumin in SMLs containing $MgFe_2O_4$ nanoparticles, before and after interaction with GUVs. **A.** SMLs of DPPC. **B.** PEGylated SMLs. Inset: Schematic representation of membrane fusion between SMLs (loaded with curcumin) and GUVs.

Concerning PEGylated SMLs, containing 95% DPPC and 5% DSPE-PEG-2000, the fluorescence anisotropy of curcumin loaded in these systems was determined as *r*=0.153 at 25° C and *r*=0.109 at 55° C. Again, the *r* values are similar to the ones measured in SMLs without PEG (Table 2). Upon interaction with GUVs, the unquenching effect of curcumin fluorescence is also detected in PEGylated SMLs (Fig. 9B) and even in a higher degree, which can indicate that the presence of PEG may facilitate the fusion of SMLs with membranes.

Overall, these results show that the aqueous and solid drug-loaded magnetoliposomes, containing superparamagnetic magnesium ferrite nanoparticles, are promising as therapeutic agents, presenting the capability of being guided with a magnetic field to the therapeutic site and release the loaded drug by fusion with the cell membrane, while allowing the simultaneous application of magnetic hyperthermia therapy. Moreover, the application of an alternating magnetic field (AMF), causing a local temperature increase by the magnetic nanoparticles, will also promote an increase in fluidity of the lipid membrane of magnetoliposomes, enhancing drug release.

Conclusions

In this work, magnesium ferrite nanoparticles with sizes around 25 nm and a superparamagnetic behaviour were synthesized. These nanoparticles were used for the preparation of magnetoliposomes, both aqueous (liposomes entrapping magnetic nanoparticles, AMLs) and solid (magnetic nanoparticles covered by a lipid bilayer, SMLs), with sizes below 130 nm.

The model drug curcumin was successfully incorporated in both AMLs and SMLs, with high encapsulation efficiencies. Fluorescence emission measurements (FRET or fluorescence quenching) indicate that curcumin-loaded AMLs and SMLs interact with models of cell membranes (GUVs) by fusion, even when PEGylation is used.

To our knowledge, it is the first time that solid and aqueous magnetoliposomes containing superparamagnetic magnesium ferrite nanoparticles were prepared and their potentialities as drug nanocarriers evaluated. These results point to future applications of magnetoliposomes containing $MgFe_2O_4$ nanoparticles in dual cancer therapy (combining magnetic hyperthermia and chemotherapy).

Authors' contributions. BDC, ISRR and FCTF performed the synthesis and structural characterization of magnetic nanoparticles, liposomes and magnetoliposomes; BDC and AROR performed the drug-loaded nanosystems and the corresponding photophysical studies; AP and AMP performed the experimental magnetic measurements; JPA supervised the determination of magnetic properties; BGA and AMP performed the analysis of results obtained by SQUID measurements and the corresponding discussion; EMSC supervised the photophysical measurements and the interpretation of results, and participated in the draft of the manuscript; PJGC conceived the study, cosupervised the photophysical measurements and wrote the final manuscript. All authors gave final approval for publication.

Competing interests. The authors declare no competing interests.

Funding. This work was supported by the Portuguese Foundation for Science and Technology (FCT) in the framework of the Strategic Funding of CF-UM-UP (UID/FIS/04650/2013). FCT, POPH-QREN and FSE are acknowledged for the PhD grant of A. R. O. Rodrigues (SFRH/BD/90949/2012).

Acknowledgements. A.R.O.R. acknowledges MAP-Fis PhD Program for support.

Ethics. It was not required to complete an ethical assessment prior to conducting this research.

Permission to carry out fieldwork. No permissions were required prior to conducting this research.

Notes and references

1 S. Mornet, S. Vasseur, F. Grasset and E. Duguet, Magnetic nanoparticle design for medical diagnosis and therapy, *J. Mater. Chem.*, 2004, **14**, 2161-2175.

2 A. S. Lübbe, C. Bergemann, J. Brock and D. G. McClure, Physiological aspects in magnetic drug targeting, *J. Magn. Magn. Mater.,* 1999, **194**, 149-155.

3 A. Hervault, N. T. K. Thanh, Magnetic nanoparticle-based therapeutic agents for thermo-chemotherapy treatment of cancer, Nanoscale 6 (2014) 11553-11573.

4 S. Dandamudi and R. B. Campbell, The drug loading, cytotoxicity and tumor vascular targeting characteristics of magnetite in magnetic drug targeting, *Biomaterials*, 2007, **28** 4673-4683.

5 S. Dandamudi and R. B. Campbell, Development and characterization of magnetic cationic liposomes for targeting tumor microvasculature, *Biochim. Biophys. Acta*, 2007, **1768**, 427-438.

6 N. Nuytten, M. Hakimhashemi, T. Ysenbaert, L. Defour, J. Trekker, S. J. Soenen, P. Van der Meeren and M. Cuyper, PEGylated lipids impede the lateral diffusion of adsorbed proteins at the surface of (magneto)liposomes*, Colloid Surf. B-Biointerfaces*, 2010, **80**, 227-231.

7 U. I. Tromsdorf, N. C. Bigall, M. G. Kaul, O. T. Bruns, M. S. Nikolic, B. Mollwitz, R. A. Sperling, R. Reimer, H. Hohenberg, W. J. Parak, S. Forster, U. Beisiegel, G. Adam and H. Weller, Size and surface effects on the MRI relaxivity of manganese ferrite nanoparticle contrast agents, *Nano Lett.,* 2007, **7**, 2422-2427.

8 E. Amstad, J. Kohlbrecher, E. Müller, T. Schweizer, M. Textor and E. Reimhult, Triggered release from liposomes through magnetic actuation of iron oxide nanoparticle containing membranes, *Nano Lett.,* 2011, **11**, 1664-1670.

9 M. M. G. Saldívar-Ramírez, C. G. Sánchez-Torres, D. A. Cortés-Hernández, J. C. Escobedo-Bocardo, J. M. Almanza-Robles, A. Larson, P. J. Reséndiz-Hernández and I. O. Acuña-Gutiérrez, Study on the efficiency of nanosized magnetite and mixed ferrites in magnetic hyperthermia. *J. Mater. Sci.: Mater. Med.,* 2014, **25**, 2229-2236.

10 Y. Wan, G. Xiong, H. Luo, F. He, Y. Huang, and X. Zhou, Preparation and characterization of a new biomedical magnesium-calcium alloy, *Mater. Des.,* 2008, **29**, 2034-2037.

11 L. Khanna and N. K. Verma, Synthesis, characterization and *in vitro* cytotoxicity study of calcium ferrite nanoparticles. *Mater. Sci. Semicond. Process.,* 2013, **16**, 1842-1848.

12 T. Maehara, K. Konishi, T. Kamimori, H. Aono, H. Hirazawa and T. Naohara, Selection of ferrite powder for thermal coagulation therapy with alternating magnetic field, *J. Mater. Sci.,* 2005, **40**, 135-138.

13 K. Sato, Y. Watanabe, A. Horiuchi, S. Yukumi, T. Doi and M. Yoshida, Feasibility of new heating method of hepatic

parenchyma using a sintered $MgFe_2O_4$ needle under an alternating magnetic field, *J. Surg. Res*., 2008, **146**, 110-116.
14 J. Chandradass, A. H. Jadhav, K. H. Kim and H. Kim, Influence of processing methodology on the structural and magnetic behavior of $MgFe_2O_4$ nanopowders, *J. Alloys Compd*., 2012, **517**, 164-169.
15 S. Kanagesan, M. Hashim, S. Tamilselvan, N. B. Alitheen, I. Ismail and G. Bahmanrokh, Cytotoxic effect of nanocrystalline $MgFe_2O4$ particles for cancer cure, *J. nanomater.,* 2013, **2013**, article 865024.
16 N. Kaur and M. Kaur, Comparative studies on impact of synthesis methods on structural and magnetic properties of magnesium ferrite nanoparticles. *Process. Appl. Ceram.*, 2014, **8**, 137-143.
17 C. Murugesan and G. Chandrasekaran, Enhanced electrical and magnetic properties of annealed magnesium ferrite nanoparticles. *J. Supercond. Nov. Magn.,* 2015, **28**, 3607-3615.
18 H. Hirazawa, S. Kusamoto, H. Aono, T. Naohara, K. Mori, Y. Hattori, T. Maehara, and Y. Watanabe, Preparation of fine $Mg_{1-x}Ca_xFe_2O_4$ powder using reverse coprecipitation method for thermal coagulation therapy in an AC magnetic field, *J. Alloy. Compd*., 2008, **4**, 467-473.
19 H. Aono, H. Hirazawa, T. Naohara and T. Maeha, Surface study of fine $MgFe_2O_4$ ferrite powder prepared by chemical methods, *Appl. Surf. Sci.* 2008, **254**, 2319-2324.
20 B. B. Aggarwal and K. B. Harikumar, Potential therapeutic effects of curcumin, the anti-inflammatory agent, against neurodegenerative, cardiovascular, pulmonary, metabolic, autoimmune and neoplastic diseases, *Int. J. Biochem. Cell Biol*., 2009, **41**, 40-59.
21 B. B. Aggarwal and B. Sung, Pharmacological basis for the role of curcumin in chronic diseases: an age-old spice with modern targets, *Trends Pharmacol. Sci.,* 2009, **30**, 85-94.
22 A. Goel, A. B. Kunnumakkara and B. B. Aggarwal, Curcumin as 'Curecumin': from kitchen to clinic, *Biochem. Pharmacol.*, 2008, **75**, 787-809.
23 J. M. Ringman, S. A. Frautschy, G. M. Cole, D. L. Masterman and J. L. Cummings, A potential role of the curry spice curcumin in Alzheimer's disease, *Curr. Alzheimer Res.*, 2005, **2**, 131-136.
24 S. Bisht, G. Feldmann, S. Soni, R. Ravi, C. Karikar, A. Maitra and A. Maitra, Polymeric nanoparticle-encapsulated curcumin ('nanocurcumin'): a novel strategy for human cancer therapy, *J. Nanobiotechnology*, 2007, **5**, article 3.
25 P. Anand, A. B. Kunnumakkara, R. A. Newman and B. B. Aggarwal, Bioavailability of curcumin: Problems and promises, *Mol. Pharm.,* 2007, **4**, 807-818.
26 S. Prasad, A. K. Tyagi and B. B. Aggarwal, Recent developments in delivery, bioavailability, absorption and metabolism of curcumin: The golden pigment from golden spice, *Cancer Res. Treat*., 2014, **46**, 2-18.
27 Y.-M. Tsai, W.-L. Chang-Liao, C.-F. Chien, L.-C. Lin and T.-H. Tsai, Effects of polymer molecular weight on relative oral bioavailability of curcumin, *Int. J. Nanomedicine*, 2012, **7**, 2957-2966.
28 C. Gong, Q. Wu, Y. Wang, D. Zhang, F. Luo, X. Zhao, Y. Wei and Z. Qian, A biodegradable hydrogel system containing curcumin encapsulated in micelles for cutaneous wound healing, *Biomaterials*, 2013, **34**, 6377-6387.
29 P. P. Dandekar, R. Jain, S. Patil, R. Dhumal, D. Tiwari, S. Sharma, G. Vanage and V. Patravale, Curcumin-loaded hydrogel nanoparticles: Application in anti-malarial therapy and toxicological evaluation, *J. Pharm. Sci*., 2010, **99**, 4992-5010.
30 A. Altunbas, S. J. Lee, S. A. Rajasekaran, J. P. Schneider and D. J. Pochan, Encapsulation of curcumin in self-assembling peptide hydrogels as injectable drug delivery vehicles, *Biomaterials*, 2011, **32**, 5906-5914.
31 J. M. H. Kremer, M. W. J. v. d. Esker, C. Pathmamanoharan and P. H. Wiersema, Vesicles of variable diameter prepared by a modified injection method, *Biochemistry*, 1977, **16**, 3932-3935.
32 K. Kirchberg, A. Becker, A. Bloesser, T. Weller, J. Timm, C. Suchomski and R. Marschall, Stabilization of monodisperse, phase-pure $MgFe_2O_4$ nanoparticles in aqueous and nonaqueous media and their photocatalytic behaviour, *J. Phys. Chem. C*, 2017, **121**, 27126-27138.
33 A. R. O. Rodrigues, I. T. Gomes, B. G. Almeida, J. P. Araújo, E. M. S. Castanheira and P. J. G. Coutinho, Magnetoliposomes based on nickel ferrite nanoparticles for biomedical applications, *Phys. Chem. Chem. Phys.*, 2015, **17**, 18011-18021.
34 A. R. O. Rodrigues, J. M. F. Ramos, I. T. Gomes, B. G. Almeida, J. P. Araújo, M.-J. R. P. Queiroz, P. J. G. Coutinho and E. M. S. Castanheira, Magnetoliposomes based on manganese ferrite nanoparticles as nanocarriers for antitumor drugs, *RSC Advances*, 2016, **6**, 17302-17313.
35 A. R. O. Rodrigues, B. G. Almeida, J. M. Rodrigues, M.-J. R. P. Queiroz, R. C. Calhelha, I. C. F. R. Ferreira, A. Pires, A. M. Pereira, J. P. Araújo, P. J. G. Coutinho and E. M. S. Castanheira, Magnetoliposomes as carriers for promising antitumor thieno[3,2-*b*]pyridin-7-arylamines: photophysical and biological studies, *RSC Advances*, 2017, **7**, 15352-15361.
36 A. R. O. Rodrigues, P. M. F Mendes, P. M. L. Silva, V. A. Machado, B. G. Almeida, J. P. Araújo, M.-J. R. P. Queiroz, E. M. S. Castanheira and Paulo J. G. Coutinho, Solid and aqueous magnetoliposomes as nanocarriers for a new potential drug active against breast cancer, *Colloid Surf. B-Biointerfaces*, 2017, **158**, 460-468.
37 Y. Tamba, H. Terashima and M. Yamazaki, A membrane filtering method for the purification of giant unilamellar vesicles, *Chem. Phys. Lipids*, 2011, **164**, 351-358.
38 T. Tanaka, Y. Tamba, S. M. Masum, Y. Yamashita and M. Yamazaki, La^{3+} and Gd^{3+} induce shape change of giant unilamellar vesicles of phosphatidylcholine, *Biochim. Biophys. Acta*, 2002, **1564**, 173-182.
39 B. Valeur, Molecular Fluorescence – Principles and Applications, Wiley-VCH, Weinheim, 2002.
40 I. Johnson and M. Spence (eds.), Molecular Probes Handbook: A Guide to Fluorescent Probes and Labeling Technologies, 11th Ed., Invitrogen, 2011.
41 A. S. Edelstein and R. C. Cammaratra, *Nanomaterials: Synthesis, Properties and Applications,* Taylor & Francis Group, New York, 1996.
42 S. Maensiri, M. Sangmanee and A. Wiengmoon, Magnesium ferrite ($MgFe_2O_4$) nanostructures fabricated by electrospinning, *Nanoscale Res. Lett.*, 2009, **4**, 221-228.
43 J. Rodriguez-Carvajal, FULLPROF: A Program for Rietveld refinement and pattern matching analysis, *Abstracts of the Satellite Meeting on Powder Diffraction of the XV Congress of the IUCr*, p. 127, Toulouse, 1990.
44 C. M. B Henderson, J. M. Charnock and D. A. Plant, Cation occupancies in Mg, Co, Ni, Zn, Al ferrite spinels: a multi-element EXAFS study, *J. Phys.: Condens. Matter*, 2007, **19**, 076214.
45 H. S. C. O'Neill, H. Annersten and D. Virgo, The temperature dependence of the cation distribution in magnesioferrite ($MgFe_2O_4$) from powder XRD structural refinements and Mössbauer spectroscopy, *Am. Mineral.*, 1992, **77**, 725-740.
46 S. Ammar, N. Jouini, F. Fiévet, O. Stephan, C. Marhic, M. Richard, F. Villain, Ch. Cartier dit Moulin, S. Brice and Ph. Sainctavit, Influence of the synthesis parameters on the cationic distribution of $ZnFe_2O_4$ nanoparticles obtained by

forced hydrolysis in polyol medium, *J. Non-Cryst. Solids*, 2004, **345-346**, 658-662.
47 O. Stenzel, The Physics of Thin Film Optical Spectra – An Introduction, Springer, Berlin, 2005.
48 A. Manikandan, J. J. Vijaya, M. Sundararajan, C. Meganathan, L. J. Kennedy, M. Bououdina, Optical and magnetic properties of Mg-doped $ZnFe_2O_4$ nanoparticles prepared by rapid microwave combustion method, *Superlattices Microstruc*., 2013, **64**, 118-131.
49 H. G. Kim, P. H. Borse, J. S. Jang, E. D. Jeong, O. S. Jung, Y. J. Suh and J. S. Lee, Fabrication of $CaFe_2O_4/MgFe_2O_4$ bulk heterojunction for enhanced visible light photocatalysis, *Chem. Comm.*, 2009, **39**, 5889-5891.
50 C. Pereira, A. M. Pereira, C. Fernandes, M. Rocha, R. Mendes, M. P. F. Garcia, A. Guedes, P. B. Tavares, J.-M. Grenèche, J. P. Araújo and C. Freire, Superparamagnetic MFe_2O_4 (M = Fe, Co, Mn) Nanoparticles: Tuning the Particle Size and Magnetic Properties through a Novel One-Step Coprecipitation Route, *Chem. Mater*., 2012, **24**, 1496-1504.
51 F. Tournus and A. Tamion, Magnetic susceptibility curves of a nanoparticle assembly. II. Simulation and analysis of ZFC/FC curves in the case of a magnetic anisotropy energy distribution, *J. Magn. Magn. Mater.*, 2011, **323**, 1118-1127.
52 R. H. Kodama, Magnetic nanoparticles, *J. Magn. Magn. Mater.*, 1999, **200**, 359-372.
53 Y. Ichiyanagi, M. Kubota, S. Moritake, Y. Kanazawa, T. Yamada and T. Uehashi, Magnetic properties of Mg-ferrite nanoparticles, *J. Magn. Magn. Mater.*, 2007, **310**, 2378-2380.
54 G. Vallejo-Fernandez, O. Whear, A. G. Roca, S. Hussain, J. Timmis, V. Patel and K. O'Grady, Mechanisms of hyperthermia in magnetic nanoparticles, *J. Phys. D: Appl. Phys.,* 2013, **46**, 312001 (6 pp).
55 T. Bala, C. R. Sankar, M. Baidakova, V. Osipov, T. Enoki, P. A. Joy, B. L. V. Prasad and M. Sastry, Cobalt and magnesium ferrite nanoparticles: Preparation using liquid foams as templates and their magnetic characteristics, *Langmuir*, 2005, **21**, 10638-10643.
56 D.-L. Zhao, X.-W. Zeng, Q.-S. Xia and J.-T. Tang, Preparation and coercivity and saturation magnetization dependence of inductive heating property of Fe_3O_4 nanoparticles in an alternating current magnetic field for localized hyperthermia, *J. Alloys Compd.*, 2009, **469**, 215-218.
57 J. Pearce, A. Giustini, R. Stigliano and P. J. Hoopes, Magnetic heating of nanoparticles: the importance of particle clustering to achieve therapeutic temperatures, *J. Nanotechnol. Eng. Med.*, 2013, **4**, 011005.
58 M. Widdrat, M. Kumari, E. Tompa, M. Pósfai, A. M. Hirt and D. Faivre, Keeping nanoparticles fully functional: Long-term storage and alteration of magnetite, *ChemPlusChem*, 2014, **79**, 1225-1233.
59 M. Kawanishi, S. Ogo, M. Ikemoto, Y. Totsuka, K. Ishino, K. Wakabayashi, T. Yagi, Genotoxicity and reactive oxygen species production induced by magnetite nanoparticles in mammalian cells, *J. Toxicol. Sci.,* 2013, **38**, 503-511.
60 G. Liu, J. Gao, H. Ai and X. Chen, Applications and potential toxicity of magnetic iron oxide nanoparticles, *Small*, 2013, **9**, 1533-1545.
61 K. C. Kwon, E. Jo, Y.-W. Kwon, B. Lee, J. H. Ryu, E. J. Lee, K. Kim and J. Lee, Superparamagnetic Gold Nanoparticles Synthesized on Protein Particle Scaffolds for Cancer Theragnosis, *Adv. Mater*., 2017, 1701146.
62 C. Jaafar-Maalej, R. Diab, V. Andrieu, A. Elaissari and H. Fessi, Ethanol injection method for hydrophilic and lipophilic drug-loaded liposome preparation, *J. Liposome Res*., 2010, **20**, 228-243.
63 R. R. Sawant and V. P. Torchilin, Challenges in development of targeted liposomal therapeutics, *AAPS J.*, 2012, **14**, 303-315.
64 H. Curtis and N. Barnes, Biology, 5th Edition, Worth Publishers, New York, 1989.
65 B. Lentz, Membrane 'fluidity' as detected by diphenylhexatriene probes, *Chem. Phys. Lipids*, 1989, **50**, 171-190.
66 Y. Manolova, V. Deneva, L. Antonov, E. Drakalska, D. Momekova and N. Lambov, The effect of the water on the curcumin tautomerism: A quantitative approach, *Spectroc. Acta Pt. A - Molec. Biomolec. Spectr.,* 2014, **132**, 815-820.
67 S. Kawano, I. Inohana, Y. Hashi and J.-M. Lin, Analysis of keto-enol tautomers of curcumin by liquid chromatography/ mass spectrometry, *Chin. Chem. Lett.,* 2013, **24**, 685-687.
68 S. M. Khopde, K. I. Priyadarsini, D. K. Palit and T. Mukherjee, Effect of solvent on the excited-state photophysical properties of curcumin, *Photochem. Photobiol.,* 2000, **72**, 625-631.
69 J. N. Israelachvili, S. Marcelja and R. G. Horn, Physical principles of membrane organization, *Q. Rev. Biophys*., 1980, **13**, 121-200.
70 D. B. Kell and C. M. Harris, On the dielectrically observable consequences of the diffusional motions of lipids and proteins in membranes. 1. Theory and overview, *Eur. Biophys. J.,* 1985, **12**, 181-197.
71 L. Tilley, K. R. Thulborn and W. H. Sawyer, An assessment of the fluidity gradient of the lipid bilayer as determined by a set of *n*-(9-anthroyloxy)fatty acids (*n* = 2, 6, 9, 12, 16), *J. Biol. Chem*., 1979, **254**, 2592-2594.
72 M. A. Bahri, B. J. Heyne, P. Hans, A. E. Seret, A. A. Mouithys-Mickalad and M. D. Hoebeke, Quantification of lipid bilayer effective microviscosity and fluidity effect induced by propofol, *Biophys. Chem.,* 2005, **114**, 53-61.
73 H. Vilaça, T. Castro, F.M.G. Costa, M. Melle-Franco, L. Hilliou, I. W. Hamley, E. M. S. Castanheira, J. A. Martins, P. M. T. Ferreira, Self-assembled dehydropeptide RGD hydrogels for drug delivery applications, *J. Mater. Chem. B,* 2017, **5**, 8607-8617.
74 P. Greenspan and S. D. Fowler, Spectrofluorometric studies of the lipid probe Nile Red, *J. Lipid Res.*, 1985, **26**, 781-789.
75 I. and G. Krishnamoorthy, Probing the link between proton transport and water content in lipid membranes, *J. Phys. Chem. B*, 2001, **105**, 1484-1488.
76 P. J. G. Coutinho, E. M. S. Castanheira, M. C. Rei and M. E. C. D. Real Oliveira, Nile Red and DCM Fluorescence Anisotropy Studies in $C_{12}E_7$/DPPC Mixed Systems, *J. Phys. Chem. B*, 2002, **106**, 12841-12846.
77 E. Feitosa, F. R. Alves, A. Niemiec, M. E. C. D. R. Oliveira, E. M. S. Castanheira and A.L.F. Baptista, Cationic liposomes in mixed didodecyldimethylammonium bromide and dioctadecyldimethylammonium bromide aqueous dispersions studied by differential scanning calorimetry, Nile Red fluorescence, and turbidity, *Langmuir,* 2006, **22**, 3579-3585.
78 J. M. Harris and R. B. Chess, Effect of PEGylation on pharmaceuticals, *Nat. Rev. Drug Discov.,* 2003, **2**, 214-221.
79 E. Illés, M. Szekeres, E. Kupcsik, I. Y. Tóth, K. Farkas, A. Jedlovszky-Hajdú and E. Tombácz, PEGylation of surfacted magnetite core-shell nanoparticles for biomedical application, *Colloid Surf. A-Physicochem. Eng. Asp.*, 2014, **460**, 429-440.
80 J. Estelrich, M. A. Busquets and M. C. Morán, Effect of PEGylation on Ligand-Targeted Magnetoliposomes: A Missed Goal, *ACS Omega*, 2017, **2**, 6544-6555.